JAAS

TECHNICAL NOTE

Cite this: DOI: 10.1039/c4ja00297k

In situ Sr isotope measurement of small glass samples using multiple-Faraday collector inductively coupled plasma mass spectrometry with 10^{12} Ω resistor high gain Faraday amplifiers†

Qing Chang,* Jun-Ichi Kimura and Bogdan Stefanov Vaglarov

An analytical protocol was developed for correcting Kr baseline-induced bias and Rb isobaric overlap factors to analyse Sr isotope ratios for small glass samples using excimer laser ablation (LA) with an Aridus II desolvating nebuliser dual-intake system and multiple collector inductively coupled plasma mass spectrometry (MC-ICP-MS). The combined use of a low-oxide interface setup, along with high-gain Faraday amplifiers with a 10^{12} Ω resistor, enabled precise determination of Sr isotope ratios from 50–100 μm diameter craters at 10 Hz laser repetition rate. Residual analytical biases of $^{84}Sr/^{86}Sr$ and $^{87}Sr/^{86}Sr$ isotope ratios, obtained from Kr baseline suppressions (Kimura *et al.*, 2013, *Journal of Analytical Atomic Spectrometry*, 28, 945–957), were found to be nonlinear, but the correction method was applicable to 50–200 μm/10 Hz craters. We also found that the $^{85}Rb/^{87}Rb$ overlap correction factor changed with time with a change in the surface condition of the sampler–skimmer cones. The correction factor of $^{85}Rb/^{87}Rb$ was thus determined at least once per five unknown measurements using the Aridus solution intake line. We determined $^{87}Sr/^{86}Sr$ isotope ratios from MkAn anorthite (Sr = 305 ppm, Rb = 0.07 ppm), BHVO-2G, KL2-G, ML3B-G (Sr = 312–396 ppm, Rb = 5.8–9.2 ppm), and BCR-2G (Sr = 337 ppm, Rb = 48.5 ppm) basalt glasses using a 50–100 μm/10 Hz crater. The results agree well with their reference values, determined by thermal ionisation mass spectrometry, even with the high Rb/Sr ratio (0.14) in the BCR-2G glass. The internal/intermediate precisions were ±0.0002 (two-standard deviation: 2SD) for 100 μm craters and ±0.0005 for 50 μm craters. The new instrument settings and analytical protocol improved the precision by a factor of two compared to the previous report using LA-(sector field)-ICP-MS and enables the analysis of sample volumes that are ten times smaller than those used in previous LA-MC-ICP-MS analyses with equal precision.

1. Introduction

1.1. *In situ* Sr isotope ratio analysis by LA-ICP-MS

In situ analysis of strontium isotopes using laser ablation multiple collector inductively coupled plasma mass spectrometry (LA-MC-ICP-MS) has been a useful geochemical tool for the analysis of plagioclase crystals or carbonate materials and glasses.[1–6] Complex isobaric overlaps from Ar gas blanks and isobaric ions, oxides, and doubly charged ions from the samples are of concern for four naturally occurring Sr isotopes, ^{84}Sr, ^{86}Sr, ^{87}Sr, and ^{88}Sr. Data correction protocols are therefore very complex, prompting rigorous examination. These problems and their resulting solutions have been summarized by Vroon *et al.*[7]

The most commonly employed Sr isotope measurement protocol[7] for the geochemical samples is the use of on-peak background subtraction, which corrects for Kr gas blanks and instrumental memories of Sr and Rb,[1,2,5,6,8–13] although iterative subtraction of the Kr baselines is also a useful technique.[3,13] Overlap correction of ^{87}Rb using ^{85}Rb is achieved by an external mass bias correction from Sr, determined as $^{86}Sr/^{88}Sr$ = 0.1194,[1,2,5,6,8–12] but is successful only with the actual determination of $^{85}Rb/^{87}Rb$, either by measurement of a Rb-doped Sr standard solution, using a solution-laser aerosol-dual intake system,[14] or by measurement of both natural and synthetic glasses with known $^{87}Sr/^{86}Sr$ isotope ratios.[2,3,15] Interference from Ca dimers, CaAr, and $^{23}Na^{60}$–^{64}Ni molecular ions is usually negligible for plagioclase crystals and carbonates.[6,7,10] Oxide interference on ^{85}Rb and ^{87}Sr from $^{69}Ga^{16}O$ and $^{71}Ga^{16}O$ is significant for samples rich in Al, such as plagioclase and glass, as Ga has a chemical affinity for Al and is highly partitioned in these samples.[14] Therefore, by using particular MC-ICP-MS settings,[16] high oxide yields are avoided.[6,10] Interference from

Department of Solid Earth Geochemistry (DSEG), Japan Agency for Marine-Earth Science and Technology (JAMSTEC), 2–15 Natsushima-Cho, Yokosuka 237-0061, Japan. E-mail: qchang@jamstec.go.jp; Fax: +81-46-867-9625; Tel: +81-46-867-9634
† Electronic supplementary information (ESI) available: Analytical results of Sr isotope ratios. See DOI: 10.1039/c4ja00297k

doubly charged rare earth element (REE) ions are also obvious,[10,12,17] and care must be taken to exclude REE-rich Sr-poor samples (e.g., clinopyroxene) and co-ablation of REE-rich mineral inclusions (e.g., apatite). The REE double charges such as $^{166}Er^{++}$, $^{168}Er^{++}$, and $^{170}Er^{++}$ for ^{83}Kr, ^{84}Sr, and ^{85}Rb, respectively, and $^{170}Yb^{++}$, $^{172}Yb^{++}$, $^{174}Yb^{++}$ and $^{176}Yb^{++}$ for ^{85}Rb, ^{86}Sr, ^{87}Sr and ^{88}Sr, respectively, can be monitored, or even corrected for, by placing the Faraday collectors at half-mass positions of $^{83.5}M$ ($^{167}Er^{++}$) and $^{86.5}M$ ($^{173}Yb^{++}$).[10,17] Finally, analytical results are obtained by the internal mass fractionation correction of Sr given that $^{86}Sr/^{88}Sr = 0.1194$.[7] Additional bias corrections for Kr baseline suppression caused by LA aerosols were recently introduced for $^{87}Sr/^{86}Sr$ measurements to further improve analytical precision and reproducibility for samples low in Sr (e.g., 300 ppm), for which large amounts of LA aerosols needed to be introduced.[14]

1.2.   Analysis of Sr isotope ratios in glass samples

Analysis of the $^{87}Sr/^{86}Sr$ isotope ratio from a small glass sample, such as olivine-hosted small glass inclusions (diameters of 50–200 μm or less), is particularly useful for the identification of the source processes in the genesis of basalt magmas. These glass inclusions can preserve information regarding the primary magma generated in the deep mantle and is unaffected by chemical modifications during ascent to the surface by encapsulation of tiny drops of the deep, quenched magmas.[3,18] Attempts to analyse basalt glass were described by Christensen et al. in the first paper published on in situ $^{87}Sr/^{86}Sr$ isotope analysis using LA-MC-ICP-MS, in which they analysed the groundmass glass of Long Valley basalt from a 300 μm/20 Hz crater (approximate sample volume: $V = \sim2.1 \times 10^{-5}$ cm^3), sampled by an infrared (IR) Nd-YAG laser with an internal/intermediate precision of $^{87}Sr/^{86}Sr =$ approximately ±0.0005 (two-standard deviation: 2SD).[1]

The attempt continued with development in an ultraviolet 213 nm YAG laser and a third-generation MC-ICP-MS, allowing analysis from a smaller crater of 120 μm/20 Hz ($V = \sim7.9 \times 10^{-7}$ cm^3) with a similar internal/intermediate precision of approximately ±0.0005 2SD.[3] An alternative approach was to use a sector field (SF)-ICP-MS with rapid peak jumping using a single ion counter (IC) connected to a 193 nm excimer laser (ExLA). This allowed analysis of a smaller sample volume, a crater from 50 μm/10 Hz ($V = \sim9.8 \times 10^{-8}$ cm^3), with an intermediate precision of approximately ±0.0010 2SD.[19] Analysis of the small sample volume was achieved through the use of the high-sensitivity IC, whereas the use of the IC with peak jumping resulted in poor intermediate precision.

1.3.   Focus

In this study, we present an improved analytical technique for Sr isotope analysis of glass samples. We apply a 193 nm ExLA laser sampling method, with simultaneous introduction of Aridus II solution aerosols (dual intake system),[14] connected to an MC-ICP-MS. In order to prevent any potential oxide interference, the interface of the MC-ICP-MS was set to achieve the lowest oxide molecular yield.[20] Low instrumental sensitivity

with the interface was accounted for by the use of a high-efficiency rotary pump at the interface[14,20–22] and the application of high-gain Faraday amplifiers using a 10^{12} Ω resistor.

The use of these amplifiers increases sensitivity by 10 times by reducing the signal-to-noise ratio to half of what would be obtained from an amplifier with a 10^{11} Ω resistor. This can in turn reduce analytical error generated during the analysis by more than half for low electron currents.[23,24] We also examine the Kr baseline-induced bias[14] during loading of smaller samples to the ICP and temporal changes in the Rb overlap correction factor for glass samples with high Rb content. The small sample size and the internal/intermediate precision achieved in this study are keys to the successful application of LA-MC-ICP-MS to small glass inclusions.

2.   Instrument setting, data acquisition/reduction

2.1.   Laser ablation (LA) and dual-intake sample introduction

The instrumentation for our LA-multiple correction (MC)-ICP-MS has been reported elsewhere for the in situ Sr isotope analysis of plagioclase crystals[14,15,25] In brief, the instrument consists of an LA-Aridus II dual-intake system including a 193 nm excimer LA system with a COMPex 102 laser source (Coherent, Göttingen, Germany) combined with an Aridus II desolvating nebuliser (CETAC Technologies, Omaha, USA). The laser aerosols in the He gas flow and the Aridus II solution aerosols in the Ar gas flow were mixed in a T-piece connector just prior to the ICP torch in the MC-ICP-MS. The excimer laser operated with a fluence of 20 J cm^{-2}, a 50–200 μm crater diameter, and, in most cases, a 10 Hz repetition rate, which resulted in craters with depths of ~50 μm after ablation for ~35 s (idle time, 10 s; data acquisition, 25 s), indicating a drilling rate of 0.125 μm per shot.

2.2.   MC-ICP-MS

A NEPTUNE MC-ICP-MS was used (Thermo Fisher Scientific, Bremen, Germany) and was modified at the interface for a high sensitivity as has been reported elsewhere.[14,20] The settings of the ion interface were normal (N) Ni sampling and normal (H) Ni skimmer cones with the guard electrode (GE) turned off (electrically disconnected) (Table 1). This allowed minimisation of the oxide molecular ion yields ($^{238}U^{16}O^+/^{238}U^+ < 1\%$, analysed in solution by Aridus II) and thus, any oxide based interference (e.g., GaO$^+$) was avoided. The important doubly charged REE ions were monitored by half mass Faradays set at $^{83.5}M$ for $^{167}Er^{++}$ and $^{86.5}M$ for $^{173}M^{++}$ (Table 1),[20] and these were almost completely absent (grand averages of the per cent REE^{++} on the most affected ^{84}Sr signals were $^{168}Er^{++}/^{84}Sr < 0\%$ and $^{168}Yb^{++}/^{84}Sr = 0.004\%$; calculations from ESI Data Table 1†) for glass samples.

With the interface designed to maintain low oxide levels, as noted above, the system sensitivity was maintained at 200 V ppm^{-1} Sr (~11 Gcps/ppm) measured from the Aridus II solution.[3,10] Analysis of ~300–400 ppm of Sr in glasses yielded a ^{88}Sr signal of 0.5–0.8 V and ~0.1–0.2 V from 100 μm/10 Hz and 50 μm/10 Hz laser craters, respectively (ESI Data Table 1†). These

Table 1 Laser and mass spectrometer set-up parameters for the LA-MC-ICP-MS Sr isotope analysis[a]

Apparatus	Experimental setting
Excimer laser	OK Laboratory Ltd. (in house)
Source wave length/pulse width	193 nm/20 ns
Energy at source	200 mJ
Focusing lens	Imaging optics using field lens and air spaced doublet objective
Spot size	50, 100, and 200 μm
Fluence at laser spot	20 J cm^{-2}
Repetition rate	10 and 20 Hz
Aridus II	CETAC Technologies
Spray chamber temperature	110 °C
Membrane temperature	160 °C
Nebuliser flow	1.0 L min^{-1}
Membrane gas flow	~3.5 L min^{-1}
Additional N$_2$ gas flow	1.5 mL min^{-1}
MC-ICP-MS	Thermo NEPTUNE
RF-power	1400 W
Guard electrode	Off (electronically disconnected)
Sampling cone	N-sample cone (Ni)
Skimmer cone	N-skimmer cone (Ni)
Plasma gas (Ar)	1.0 L min^{-1}
Laser carrier gas (He)	0.7 L min^{-1}
Interface vacuum with E2M80	1.7 mbar with He ablation carrier gas
Acquisition time	0.5 s × 50 scans for LA and 4 s × 50 scans for solution
Faraday detector setting	
^{83}Kr (^{83}Kr, ^{43}Ca^{40}Ca, ^{43}Ca^{40}Ar)	FC L4 (10^{11} Ω amplifier)
$^{83.5}$M (^{167}Er^{++})	FC L3 (10^{11} Ω amplifier)
^{84}Sr (^{84}Kr, ^{44}Ca^{40}Ca, ^{44}Ca^{40}Ar)	FC L2 (10^{12} Ω amplifier)
^{85}Rb (^{85}GaO)	FC L1 (10^{12} Ω amplifier)
^{86}Sr (^{86}Kr, ^{46}Ca^{40}Ca, ^{46}Ca^{40}Ar)	FC Center (10^{12} Ω amplifier)
$^{86.5}$M (^{173}Yb^{++})	FC H1 (10^{11} Ω amplifier)
^{87}Sr (^{87}Rb, ^{85}GaO)	FC H2 (10^{12} Ω amplifier)
^{88}Sr (^{48}Ca^{40}Ca, ^{48}Ca^{40}Ar)	FC H3 (10^{12} Ω amplifier)
Background subtraction	On peak background subtraction

[a] FC: Faraday cup; isobaric atomic and molecular ions are shown in parentheses.

values were sufficient for an internal analytical precision of ^{87}Sr/^{88}Sr = ±0.0002 to ~0.0010 (2SE) after ~25 s of data acquisition. This was achieved by the application of high-gain Faraday amplifiers, equipped with 10^{12} Ω resistors,[23] to all naturally occurring Sr isotopes (^{84}Sr, ^{86}Sr, ^{87}Sr, and ^{88}Sr) and ^{85}Rb (Table 1).

2.3. Laser ablation protocol

We especially focused on optimizing the LA analytical protocol for the use of 10^{12} Ω high-gain amplifiers because of their slow response to transient signals.[23,26] One cycle of data acquisition consisted of: (1) two 30 s baseline measurements made on-peak before laser firing; (2) subsequent firing of the laser for 10 s without data acquisition, allowing stabilisation of the LA signal and the current applied to the Faraday amplifiers in order to avoid the acquisition of transient signals during LA signal growth; and (3) data acquisition for ~25 s using a time slice of ~0.524 s for 50 scans, completed while the signal output was flat and stable (Fig. 1). The detailed setup parameters of the

laser system and the MC-ICP-MS, including the Faraday collector setup in the mass spectrometer, are listed in Table 1.

2.4. Correction of Rb isobaric overlap

A correction of interference from the ^{87}Rb isobar on ^{87}Sr is particularly important in the precise analysis of glasses because natural basaltic glasses contain Rb in the range 0.02–0.15 or more times the amount of Sr.[19,27] Previous studies used both synthetic[2] or natural glasses[3,19] of known contents of Rb and Sr and of known ^{87}Sr/^{86}Sr isotope ratios. This allows determination of the overlap correction factor of Rb by adjusting the ^{85}Rb/^{87}Rb isotope ratios to reproduce the known ^{87}Sr/^{86}Sr isotope ratio of the glasses.

We have been using a different approach for determination of the Rb overlap correction factor, using a LA–Aridus solution aerosol dual-intake system. This system has been applied to Hf, Nd, and Sr isotope analyses of zircon,[28] monazite/apatite and rutile,[20] and plagioclase,[14] respectively. The advantage of this method is its ability to simultaneous fine-tune the MC-ICP-MS instrument for both the solution and the LA aerosols from the
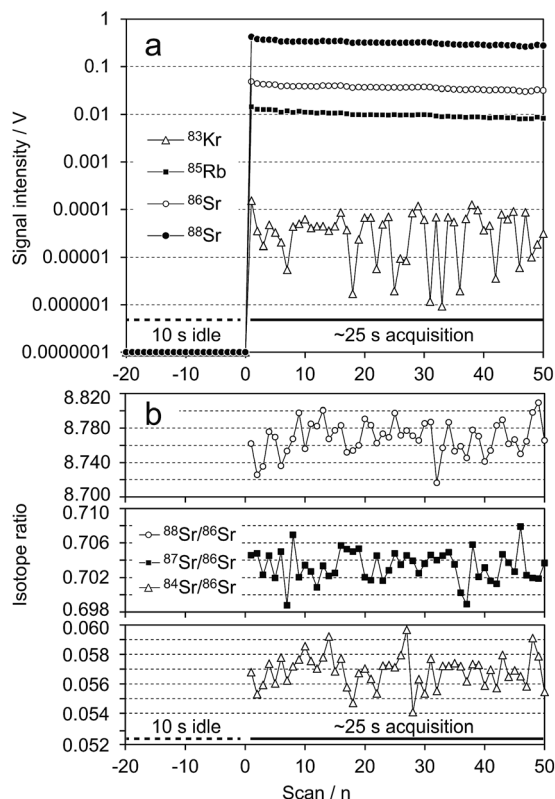
Fig. 1 Signal profiles (a) and isotope ratios (b) acquired from a 50 μm crater in ~25 s on BCR-2G. Stable signals and isotope ratios are obtained after 10 s of idle time with laser firing. No effect from the slow response of the Faraday amplifiers was observed.

dual-intake lines, by using solution aerosols while LA firing is off and the laser cell gas is on. Precise determination of an overlap correction factor (*e.g.*, [176]Yb and [176]Lu on [176]Hf;[28] [144]Sm on [144]Nd;[20] and [87]Rb on [87]Sr[14]) is simple by using mixed solutions with known (not necessarily accurate) concentrations of the interfering-interfered elements and known isotope composition.

The tuning solution can easily be prepared by mixing standard solutions. The determined correction factor can be used for the LA aerosols while Aridus II introduces deionised water (DIW). The matrix effect of the concomitant major elements from LA aerosols has been examined by major element-doped solutions[28] or by comparisons to the known TIMS values of the LA analytes.[14,20,28] The bias was found to be negligible within the level of intermediate precision of ±0.00002 for Hf (~90 ppm offset in naturally occurring [176]Hf/[177]Hf), Nd (~40 ppm offset in [143]Nd/[144]Nd), and Sr (~30 ppm offset in [87]Sr/[86]Sr) isotope analyses.[14,20,28] It should be noted that the majority of these analyses were mostly done with a crater size smaller than 200 μm/20 Hz and with the same instruments used in this study. The effectiveness and stability of Rb overlap correction are discussed in Section 3.2, particularly for glass samples high in Rb content.

2.5. Data reduction

First, the peak intensities of [84]Sr, [86]Sr, [87]Sr, [88]Sr, and [85]Rb were measured using on-peak background subtraction. [87]Sr intensity

was corrected for [87]Rb overlap by using the pre-determined [85]Rb/[87]Rb isotope ratio (Section 2.4) and the measured [85]Rb intensity. [84]Sr/[86]Sr and [87]Sr/[86]Sr isotope ratios were calculated from the intensities of [84]Sr, [86]Sr and [87]Sr (employing the correction for [87]Rb overlap), while [88]Sr was determined by the exponential law given that [86]Sr/[88]Sr = 0.1194. Further Kr baseline bias was corrected by using [84]Sr/[86]Sr and [87]Sr/[86]Sr ratios with the following equation:

$$^{87}Sr/^{86}Sr_{corrected} = {}^{87}Sr/^{86}Sr_{original}/(-0.14121 \times {}^{84}Sr/^{86}Sr + 1.0081)$$

Using the empirical correction coefficients proposed by Kimura *et al.*[14] The above calculations were applied off-line to all 50 scans in a given run. An average and twice the standard error (2SE) were calculated for each spot; in this case, all the errors that propagated from each isotope measurement were included in the calculated 2SE, while errors from the Rb overlap correction factor and the coefficients used for Kr baseline bias were not included because of their minimal effect.

Kr bias correction itself does not improve internal or external precision caused by the short or long term drift in Kr baselines, a feature that is described elsewhere for iterative Kr baseline subtraction.[13] The major role of this technique is to account for Kr baseline suppression due to the mass loading of LA aerosols; the improvement in this bias can be as high as 250 ppm, which is far greater than the Kr baseline drift.[14] The effect of the Kr baseline bias with regard to this study is discussed in Section 3.1.

3. Results

Although the analytical protocol for Sr isotope measurements using LA-MC-ICP-MS has been rigorously examined and researchers have been largely in consensus regarding the analytical protocol; special care must nevertheless be taken with Kr baseline suppressions and the Rb overlap correction. We identified new features of these factors, as described below.

3.1. Kr baseline suppression with varied sample loadings

3.1.1. Mass loading and Kr baselines: a basic test. We tested the effect of mass loading of LA aerosols by analysing an ~5 ppb SRM 987 Sr standard solution, along with introduction of LA aerosols at different laser crater sizes obtained from an olivine crystal in a picrite lava from St. Helena Island.[29] The SRM 987 is free from any interference from concomitant elements, while Sr and Rb signals from the tested olivine were both below the detection limits. Kr outgassing during LA was reported from olivine in the JP-1 peridotite[14] but this was not detected from the olivine in the picrite. The olivine sample is therefore suitable for mass loading tests.

The [88]Sr intensity from ~5 ppb SRM 987 was ~0.5 V, which was approximately the same signal size as that from a 100 μm/10 Hz carter on a plagioclase/glass containing ~300 ppm Sr. The SRM 987 solution was first analysed for [87]Sr/[86]Sr without LA firing. Subsequent analyses used 50 μm/10 Hz (the rate of LA aerosol loading: Vt = 2.5 × 10⁻⁹ cm³ s⁻¹), 100 μm/10 Hz (Vt = 9.8 × 10⁻⁹ cm³ s⁻¹), 200 μm/10 Hz (Vt = 3.9 × 10⁻⁸ cm³ s⁻¹),

and 200 μm/20 Hz ($V_t = 7.8 \times 10^{-8}$ cm³ s⁻¹) craters with increasing loaded mass from the olivine aerosols. The Sr signals vary with different LA aerosol loadings when analysing a Sr-bearing material with a different crater size; therefore, the absolute role of Kr baseline suppression cannot be tested, particularly for small aerosol loading due to large internal analytical errors in $^{87}Sr/^{86}Sr$ (see Section 3.1.2).

Analytical results are given in Fig. 2. The results show a nonlinear relationship, indicating a small suppression of the Kr baseline with 50–100 μm/10 Hz craters, whereas an obvious increase in the uncorrected Sr isotope ratio occurs in 200 μm/10–20 Hz craters. This confirmed the necessity for correction of the Kr baseline suppression. The first report of this suppression was on a 200 μm/5–10 Hz crater for plagioclase analysis,[14] the necessity of which may have been questioned, but our new analysis clearly demonstrates the necessity of the correction when the sample loading of LA is greater than 3.9×10^{-8} cm³ s⁻¹. Even with low mass loading, corrected data are closer to the reference value of SRM 987, indicating the importance of this bias correction (Fig. 2).

The baseline bias correction with the heaviest sample loading at 7.8×10^{-8} cm³ s⁻¹ from a 200 μm/20 Hz crater appears to be invalid, showing a large offset in the corrected Sr isotope ratio (Fig. 2). In this particular analysis, we saw ~10% suppression of the ^{88}Sr signal for the SRM 987 solution during loading of the olivine LA aerosols, suggesting suppression of Sr in the ICP (not shown). This was not observed with the smaller sample loading. The nonlinear response of the Sr signal might originate from the nonlinear response described by Saha's equation[30,31] where an increase in the electron number density causes a sigmoidal decrease of the ionisation efficiency.[21,30–32] Sr signal suppression relative to Kr was not taken into account for the Kr baseline bias correction in the previous paper;[14] therefore, the proposed correction could apply only to the LA aerosol loading smaller than 7.8×10^{-8} cm³ s⁻¹ with the 200 μm/20 Hz crater used in this study. The effect of signal suppression is discussed further in Section 3.2.1.

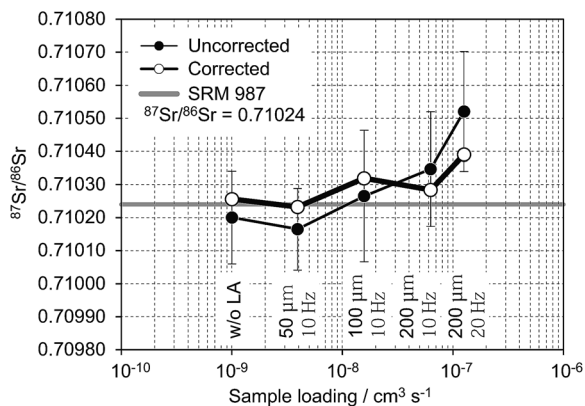**Fig. 2** Variation of $^{87}Sr/^{86}Sr$ of SRM 987 solution (~0.5 V ^{88}Sr) measured with various amounts of aerosol loading from a St Helena olivine crystal. The bias from Kr baseline suppression is significant in the crater size 200 μm/20 Hz. Uncorrected values are from isobaric overlap and mass fractionation corrections only. Corrected values are further corrected for Kr baseline-induced bias. Errors are in 2SE. Aerosol loading without LA (w/o LA) is provisionally plotted at 1×10^{-9} cm³ s⁻¹.

3.1.2. Effect of Kr baseline suppression in plagioclase analysis. We conducted a series of experiments using an extremely homogeneous anorthite plagioclase MkAn.[14,25] The Sr isotope composition of the crystal is homogeneous, $^{87}Sr/^{86}Sr = 0.70345 \pm 0.00002$ (error in 2SD, $n = 4$) confirmed by TIMS and LA-MC-ICP-MS.[14,25] This crystal contains minuscule amounts of Rb (0.07 ppm), with Sr = 305 ppm[21] and thus it is the best suited for examination of the Kr baseline suppression without considering the effect of Rb overlap.

Using the MkAn, analyses of Sr isotope ratios were performed with ablation conditions of 200 μm/20 Hz, 200 μm/10 Hz, 100 μm/10 Hz, and 50 μm/10 Hz (Fig. 3a and ESI Data Table 1†). We rearranged the data using the Kr baseline bias uncorrected data of $^{87}Sr/^{86}Sr$ and $^{84}Sr/^{86}Sr$ based on the crater size (Fig. 3b). The data from the 200 μm/10–20 Hz plot on the same negatively sloped linear regression line, which is sub-parallel to the theoretical fractionation line of Kr baseline suppression proposed by the previous study.[14] The amount of LA aerosols from a 200 μm/20 Hz crater is about 0.7 times smaller than that from olivine because of the poorer coupling of 193 nm excimer laser light to the transparent (Fe- and Mg-poor) plagioclase. This would be the reason for the lack of offset from the Kr baseline bias for this sample amount. In contrast, the regression lines of the 100 μm/10 Hz and 50 μm/10 Hz data are sub-parallel, but with shallower slopes than those from 200 μm craters. Kr baseline corrections, made by the theoretical model of Kimura et al.,[14] resulted in an almost flat regression line for the data from 200 μm craters (Fig. 3c), indicating almost perfect correction of the bias. The same correction made for the data from 100–50 μm craters showed slight over-reductions as shown by the positively sloped regression lines in Fig. 3c.

This examination clearly indicates that the Kr baseline suppression is due to mass loading of the plagioclase aerosols, but the degree of suppression could be nonlinear against the amount of aerosol loaded. The mass loading from 200 μm craters clearly showed the bias, whereas 50–100 μm craters showed the same bias, but to an apparently smaller extent. The systematic errors from the potential nonlinearity, deduced from the slopes of the regression lines of 50–100 μm craters, are well within the typical internal precision of ±0.0002 for these small craters both before and after the bias corrections (Fig. 3b and c). Therefore, we corrected for the baseline bias even for the small 50–100 μm craters. As shown, $^{87}Sr/^{86}Sr$ form SRM 987 solution showing a closer match to the reference value after the bias correction for a small aerosol loading (Fig. 2), which also supports our approach. The analytical results of MkAn are shown in Fig. 3a and ESI Data Table 1,† and show an almost perfect match with the isotope ratios measured by TIMS ($^{87}Sr/^{86}Sr = 0.70345 \pm 0.00002$) for all sample sizes; 0.7035 ± 0.0002, 2SD, $n = 26$, 200 μm craters; 0.7034 ± 0.0002, 2SD, $n = 10$, 100 μm craters; and 0.7035 ± 0.0008, 2SD, $n = 40$, 50 μm craters.

3.2. Rb overlap correction factor and its temporal drift

3.2.1. Determination of the Rb correction factor. We determined the $^{85}Rb/^{87}Rb$ correction factor using the dual-intake system over the period of analyses of this study and
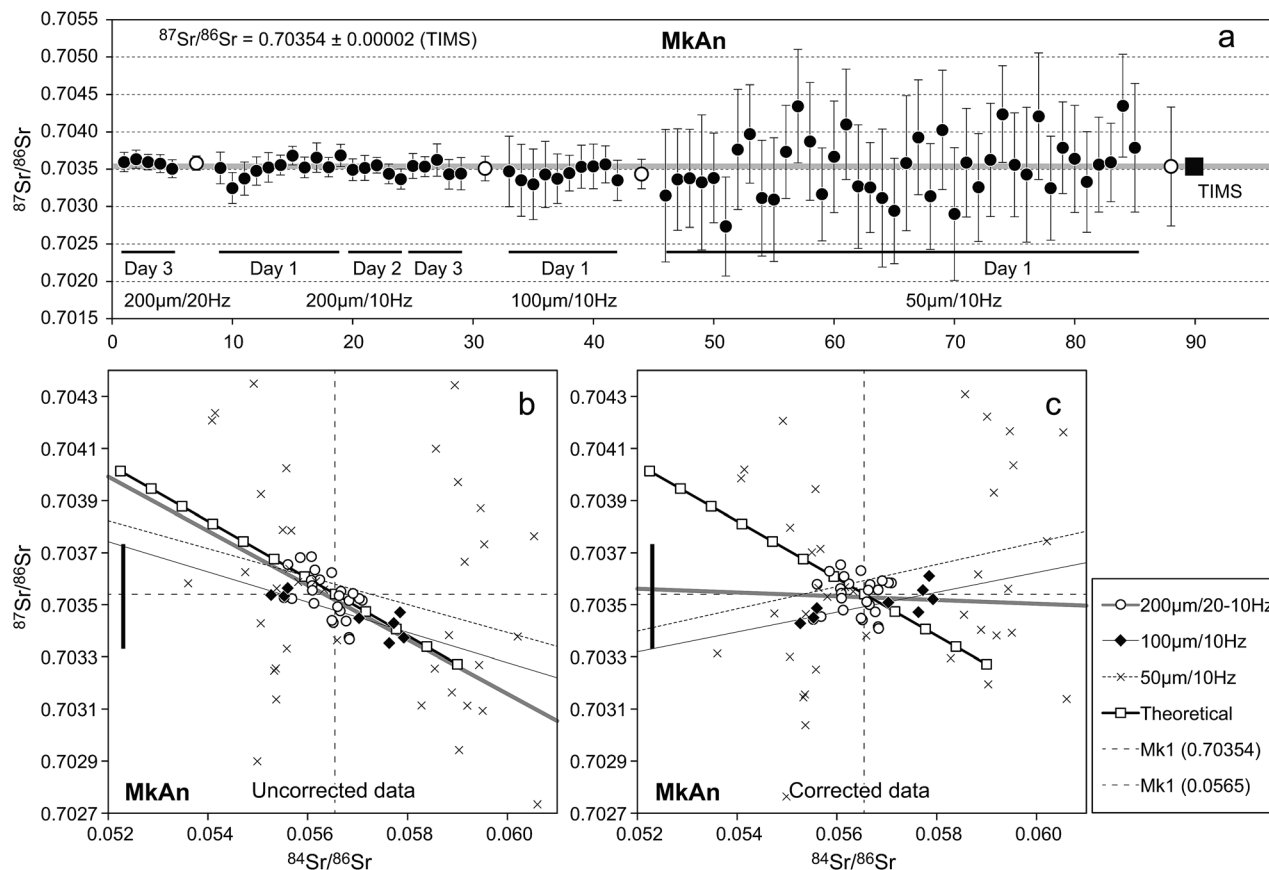
Fig. 3   Analytical results of the MkAn anorthite using different crater sizes for different amounts of sample aerosol loading (panel a). Uncorrected (panel b) and corrected $^{87}Sr/^{86}Sr–^{84}Sr/^{86}Sr$ ratios (panel c) of the Kr baseline-induced biases are compared for the different sample volumes. Data from large volume aerosols (200 μm/10–20 Hz crater) is plotted on the theoretical fractionation line of the Kr baseline suppression, while those from the smaller volume aerosols (100–50 μm/10 Hz craters) show slight over-corrections. Potential biases from these overcorrections are less than ±0.00020 (thick vertical line), well below the in-run analytical precisions for these data. Thick shaded lines, thin solid lines, and thin dotted lines are regression lines for the results from 200-, 100-, and 50 μm craters, respectively. Thin dashed lines show the reference value of the MkAn as measured by TIMS.

found a temporal change of the value obtained (Fig. 4a and b). The correction factor was obtained by analysing an ∼5 ppb NIST SRM 987 standard solution ($^{87}Sr/^{86}Sr = 0.71024$) (ref. 27) doped with an ∼1 ppb Rb, in which Rb/Sr = ∼0.2 is higher than all target glasses. The acquisition was done by the same protocol as for the LA analysis but with a longer time slice of ∼4.25 s for 50 scans in order to obtain high-precision results. In this measurement, instrumental mass fractionation of Sr was determined by a stable isotope ratio of $^{86}Sr/^{88}Sr = 0.1194$.[33] The mass fractionation was corrected by the exponential law for both Sr and Rb isotope ratios, assuming the same mass fractionation factor over the mass range $^{84}M–^{88}M$. This calculation protocol is the same as that used for the LA analyses.

We determined the $^{87}Sr/^{86}Sr = S_1$ ratio of the mixed solution with a provisional $^{85}Rb/^{87}Rb$ value (e.g., 2.5926, the canonical value of $^{85}Rb/^{87}Rb$ from the IUPAC isotopic abundances of $^{85}Rb = 72.165$ and $^{87}Rb = 27.835$).[33] The obtained $^{87}Sr/^{86}Sr$ was always incorrect because of the difference between the real and the given $^{85}Rb/^{87}Rb$ ratio, due to the different elemental sensitivity between Rb and Sr, which altered the ratio of $^{87}Rb/^{87}Rb$ (see a similar example between Sm and Nd).[20,34] The second cycle of the

calculation was done using the same analytical data with a different $^{85}Rb/^{87}Rb$ value (e.g., 2.470) to obtain the second $^{87}Sr/^{86}Sr = S_2$ ratio. The correct $^{85}Rb/^{87}Rb = R_{Rb}$ ratio should be on the linear regression line passing through the coordinates (X, Y) = (S_1, 2.5926) and (S_2, 2.470), obtaining R_{Rb} at (0.70124, R_{Rb}) for the Rb doped SRM 987 standard solution. R_{Rb} does not represent its natural value but represents the value including the correction factor (see a similar example between Lu, Yb, and Hf).[28]

3.2.2. Possible origin of enhanced Rb correction factor. The averaged $R_{Rb} = {}^{85}Rb/^{87}Rb$ value on Day 5 was 2.4688 (Fig. 4b), expressed as a mass fractionation factor of $\Delta M(Rb) = 2.417\%$ in comparison with the canonical value of $^{85}Rb/^{87}Rb = 2.5926$.[33] This fractionation factor is systematically larger than that measured for $^{86}Sr/^{88}Sr$ which gave $\Delta M(Sr) = 2.317\%$ assuming $^{86}Sr/^{88}Sr = 0.1194$ (Fig. 4c). This is due to the difference in elemental sensitivity between Rb and Sr as noted in Section 3.2.1, showing a 4.35% enhancement of Rb relative to Sr. Note that the $\Delta M(Rb)$ values in Fig. 4c are derived from the measured and interpolated values shown in Fig. 4b; the values have therefore been corrected for a temporal drift (see Section 3.2.3).
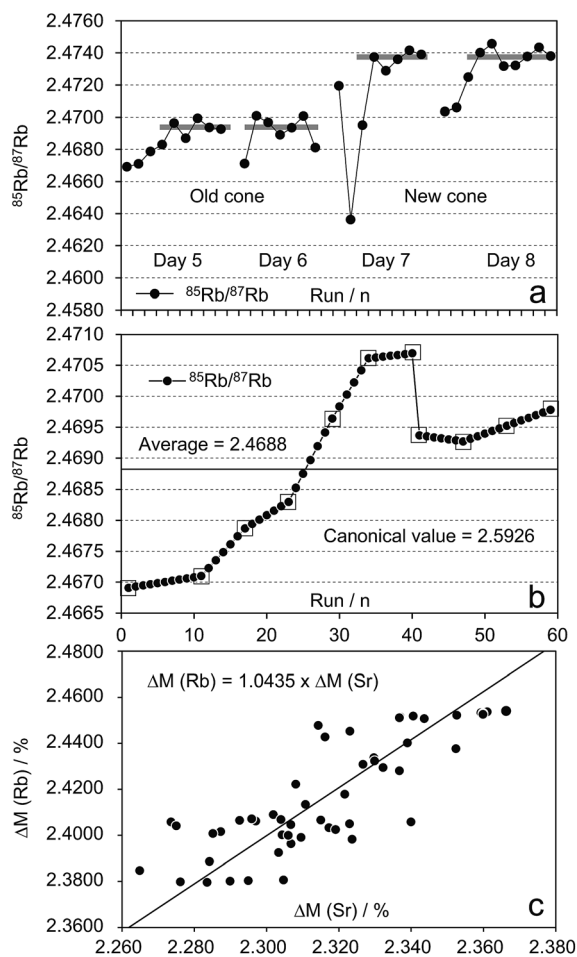
Fig. 4 Daily temporal variations of ^{85}Rb/^{87}Rb correction factors during analyses of basalt glass samples (panel a). The large gap between runs 39 and 40 is due to a long break for 2 h indicating a reverse shift of the drift due to no loading of the laser aerosols (panel b). Apparent Rb mass bias and actual Sr mass bias, measured on Day 5 (panel c). Note that open squares show measured values and dots are interpolations in panel b. See details in the text.

The enhanced ΔM(Rb) values are consistent with the higher ionisation efficiency of Rb than Sr in the ICP, where the first ionisation energy of Rb (640 kJ mol^{-1}) is lower than Sr (660 kJ mol^{-1}), and the boiling and dissociation temperatures of Rb (312.2 and 961 K, respectively) are both lower than those of Sr (1042 and 1657 K, respectively) promoting together the higher ionization efficiency of Rb than for Sr.[35] When the local plasma equilibrium of Saha's equation[30,31] and the electron number density $n_e = 1.47 \times 10^{20}$ m^{-3} are assumed, the plasma temperature at $T = 5514$ K is calculated to yield a 4.35% enhancement in the ionization efficiency of Rb (92.05%) relative to Sr (88.21%). This temperature is far lower than that of a standard ICP ($T = 6680$ K),[36] but is still similar to the apparent ionization temperature ($T = \sim5500$ K) estimated for element fractionation between a refractory SRM 612 glass and a more easily ionized BCR-2G basalt glass (see Fig. 2F in Kimura and Chang).[21] The large particle size of LA aerosols (10–500 nm with $\sim$100 nm median diameter)[21,37] and the short transit time in the

ICP may be the source of this apparently low ionization temperature.[21]

It is worth noting that the ^{85}Rb/^{87}Rb factor determined by the solution aerosols should differ from that for the LA aerosols owing to the change in the plasma conditions when the mass loading of the LA aerosols occurs.[21,32] This was not the case with the volume of LA aerosols and the internal/intermediate precision being dealt with in this study, or in our previous studies, as shown by the intermediate level of analytical precision of the standard materials (Sections 3.1.1 and 3.3). In the case of heavy mass loading, however, determination of the ^{85}Rb/^{87}Rb factor by LA aerosols should be recommended.

Finally, the clear correlation between ΔM(Rb) and ΔM(Sr) (Fig. 4c) confirms that the Rb overlap correction factor of ^{85}Rb/^{87}Rb, no matter the determination method, should be used in combination with the ^{86}Sr/^{88}Sr mass fractionation factor in each analytical run (see Section 1.1) Nevertheless, a temporal drift in the Rb correction factor occurs regardless (Fig. 4b), and should be closely monitored, determined, and applied (Section 3.2.3).

3.2.3. Temporal drift of the Rb correction factor. The ^{85}Rb/^{87}Rb correction factor drifted with time, most likely reflecting a temporal change in elemental sensitivity between Rb and Sr. The general trend showed a rapid increase in ^{85}Rb/^{87}Rb with time after the plasma was on (Fig. 4a). The drift stabilised after 2–3 h but problematic changes could have occurred (see Days 5 and 7 in Fig. 4a). The absolute ^{85}Rb/^{87}Rb value changed with different sampler and skimmer cones as shown for Days 7 and 8 in Fig. 4a. In more detail, the change showed a continuous increase from 2.4669 to 2.4706 and dropped to 2.4694 between runs 39 and 40, followed by a further increase to 2.4698 on Day 5 (Fig. 4b). The sudden drop correlates to a longer interval of 1 h with no introduction of LA aerosols. We interpreted the increase in the ratio as being caused by the change in the surface conditions of the interface cones. This daily trend is common to all examples and is significant when using a new sampler-skimmer cone for the first time (Day 7 in Fig. 4b). It is likely that the systematic difference between the cones (Day 5–6 and Day 7–8 in Fig. 4a) results from their different geometries.

The change of the ^{85}Rb/^{87}Rb factor from 2.4669 to 2.4706 causes a systematic bias increase of ^{87}Sr/^{86}Sr = 0.0014 for BCR-2G (337 ppm Sr, 48.5 ppm Rb, Rb/Sr = 0.144) and ^{87}Sr/^{86}Sr = 0.0002 for BHVO-2G (396 ppm Sr, 9.2 ppm Rb, Rb/Sr = 0.023). Considering the temporal change of the factor, frequent measurement of ^{85}Rb/^{87}Rb is crucial for glass samples with a high Rb content. We used the same, $\sim$5 ppb Sr SRM 987 solution doped with $\sim$1 ppb Rb for this purpose and determined the ^{85}Rb/^{87}Rb factors for every five unknown LA analyses. The temporal change in ^{85}Rb/^{87}Rb was the linearly interpolated for the five unknown calculations.

3.3. Analyses of basalt glass samples

With the instrument settings and the analytical protocols described in the above sections, we then analysed the BHVO-2G, KL2-G, ML3B-G, and BCR-2G glasses, which have also been

analysed in the previous LA-ICP-MS studies[18,19] and TIMS reference values are thus available.[27]

The basalt glasses of BHVO-2G (basalt from the Hawaiian Volcano Observatory), KL2-G (from Kilauea volcano), and ML3B-G (from Mauna Loa volcano) are all from the Big Island of Hawaii. As shown in Table 2 and ESI Data Table 1,† the results of BHVO-2G were: $^{87}Sr/^{86}Sr = 0.70345 \pm 0.00020$ ($n = 15$) from 100 μm/10 Hz craters and 0.7035 ± 0.0005 ($n = 55$) from 50 μm/10 Hz craters, for the TIMS value of $^{87}Sr/^{86}Sr = 0.703469 \pm 0.000010$ (Fig. 5a); those of KL2-G were: $^{87}Sr/^{86}Sr = 0.70352 \pm 0.00013$ ($n = 5$) from 100 μm/10 Hz craters for the TIMS value of 0.703517 ± 0.00002; and those of ML3B-G were: $^{87}Sr/^{86}Sr = 0.70386 \pm 0.00027$ ($n = 10$) from 100 μm/10 Hz craters for the TIMS value of 0.703805 ± 0.000020. The LA results are all in

excellent agreement with the TIMS values, indicating that the appropriate correction factor was used in this study.

BCR-2G (Columbia River Basalt) glass, with Rb/Sr = 0.144, is the most difficult sample for analysis of the isobaric corrections of the concomitant Rb in this study. The results of BCR-2G also showed excellent agreement with the TIMS reference value of $^{87}Sr/^{86}Sr = 0.705000 \pm 0.000020$,[27] as shown by $^{87}Sr/^{86}Sr = 0.70495 \pm 0.00040$ ($n = 39$) from 100 μm/10 Hz craters and $^{87}Sr/^{86}Sr = 0.7051 \pm 0.0008$ ($n = 50$) from 50 μm/10 Hz craters (Fig. 5b). This proves that the method can be applied to many natural basalt melts of interests.[3]

The intermediate precisions were ± 0.00010 for 200 μm/10 Hz craters, ± 0.00013–0.00040 for 100 μm/10 Hz craters, and ± 0.00050–0.00080 for 50 μm/10 Hz craters (Table 2 and Fig. 5).

Table 2 Representative LA-MC-ICP-MS analytical results of Sr isotope ratios in synthetic glass standards[a]

Sample	Sr ppm	Rb ppm	Rb/Sr	$^{87}Sr/^{86}Sr$ LA-ICP-MS (100 μm)	2SD	n	$^{87}Sr/^{86}Sr$ LA-ICP-MS (50 μm)	2SD	n	$^{87}Sr/^{86}Sr$ TIMS	2SE (GeoREM)	Reference
BHVO-2G	396	9.2	0.023	0.70345	0.00020	15	0.7035	0.0005	55	0.703469	0.00001	This study
				—	—	—	0.7035	0.0010	36	—	—	Jochum *et al.* (2009)
				—	—	—	0.7035	0.0010	—	—	—	Sovolev *et al.* (2011)
KL2-G	356	8.7	0.024	0.70352	0.00013	5	—	—	—	0.703517	0.00002	This study
				—	—	—	0.7036	0.0008	43	—	—	Jochum *et al.* (2009)
				—	—	—	0.7035	0.0008	—	—	—	Sobolev *et al.* (2011)
ML3B-G	312	5.8	0.019	0.70386	0.00027	10	—	—	—	0.703805	0.00002	This study
				—	—	—	0.7038	0.0008	48	—	—	Jochum *et al.* (2009)
				—	—	—	0.7038	0.0010	—	—	—	Sobolev *et al.* (2011)
BCR-2G	337	48.5	0.144	0.70495	0.00040	39	0.7051	0.0008	50	0.705000	0.00002	This study

[a] Note: 2SD = two-standard deviation; 2SE = two-standard error; n = number of analyses. TIMS reference values are from GeoREM.[27]
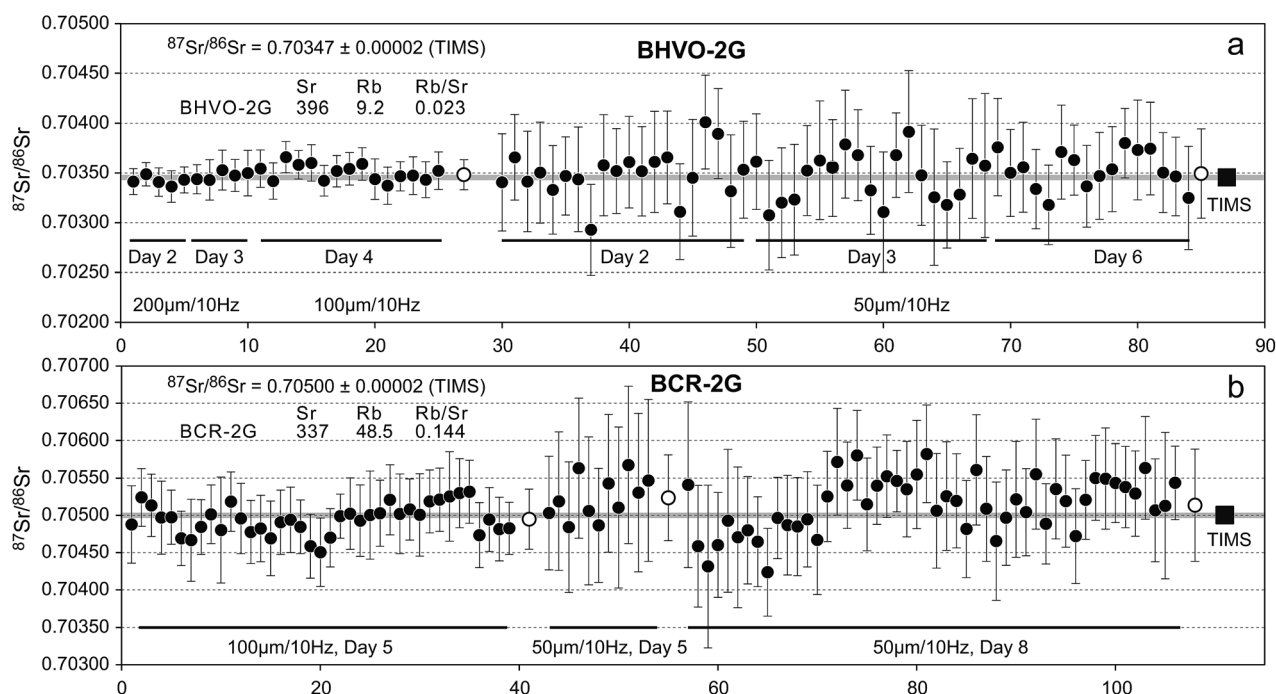

Fig. 5 Analytical results of BHVO-2G and BCR-2G glass standards. Internal precisions are given by 2SE, whereas those for averages (open circles) are given by two-standard deviation (2SD). Solid squares and shaded lines are TIMS reference values.

These internal/intermediate precisions are a factor of approximately two smaller than those obtained by LA-SF-ICP-MS for a 50 µm/10 Hz crater in year 2009.[18,19] The intermediate precisions of ±0.00050–0.00080 for a 50 µm/10 Hz crater are comparable to those obtained for a 120 µm/20 Hz crater using 216 nm YAG-LA-MC-ICP-MS in year 2006 (ref. 3) but from an ∼10 times smaller sample volume. If compared with the first report of 1064 nm by YAG-LA-MC-ICP-MS in year 1995,[1] the necessary sample amount for a ±0.00010 internal/intermediate precision is ∼200 times smaller, reflecting significant improvements in both the instruments and the analytical protocols. These improvements are useful for the analyses of small melt inclusions.

4. Conclusions

We evaluated analytical protocols using LA-MC-ICP-MS for accurate Sr isotope analysis of small glass samples. The Kr baseline suppression during LA analysis was found to be nonlinear; small for small sample aerosol loading and large for an extreme sample loading. We corrected the baseline bias for all sample amounts from the LA crater of 50–200 µm/ 10 Hz and found it to be applicable over the range. Precise Rb overlap correction using a Rb-doped standard solution and temporal variation of the correction factor were also examined. The results showed that frequent measurement of the correction factor was required for a high Rb content basalt glass. These correction methods were applied to the *in situ* Sr isotope analyses of the basalt glass standards of BHVO-2G, BCR-2G, KL2-G, and ML3B-G. The internal/intermediate precisions achieved for the glass standards were $^{87}Sr/^{86}Sr = \pm 0.00010$ (200 µm/10 Hz) to 0.00080 (50 µm/10 Hz), dependent on the crater size and Rb content. The results were a factor of two more precise than the previous method using a 50 µm crater with ExLA-SF-ICP-MS and were achieved with a ten times smaller sample volume than those in 213 nm Nd-YAG-MC-ICP-MS. The results demonstrate the wide application of this method to many naturally occurring melt inclusions in olivine, which typically have a diameter of 30–200 µm with Sr levels of 200–300 ppm.

Acknowledgements

References

1 J. N. Christensen, A. N. Halliday, D.-C. Lee and C. M. Hall, *Earth Planet. Sci. Lett.*, 1995, **136**, 79–85, DOI: 10.1016/0012-821x(95)00181-6.

2 J. Davidson, F. Tepley III, Z. Palacz and S. Me¡an-Main, *Earth Planet. Sci. Lett.*, 2001, **184**, 427–442.

3 M. G. Jackson and S. R. Hart, *Earth Planet. Sci. Lett.*, 2006, **245**, 260–277, DOI: 10.1016/j.epsl.2006.02.040.

4 T. Takahashi, Y. Hirahara, T. Miyazaki, B. S. Vaglarov, Q. Chang, J.-I. Kimura and Y. Tatsumi, *JAMSTEC Report R&D*, 2009, **Special Issue**, 59–64.

5 M. McCulloch, M. Cappo, J. Aumend and W. Müller, *Mar. Freshwater Res.*, 2005, **56**, 637–644, DOI: 10.1071/mf04184.

6 J. Woodhead, S. Swearer, J. Hergt and R. Maas, *J. Anal. At. Spectrom.*, 2005, **20**, 22–27.

7 P. Z. Vroon, B. van der Wagt, J. M. Koornneef and G. R. Davies, *Anal. Bioanal. Chem.*, 2008, **390**, 465–476, DOI: 10.1007/s00216-007-1742-9.

8 R. Barnett-Johnson, F. C. Ramos, C. B. Grimes and R. B. MacFarlane, *Can. J. Fish. Aquat. Sci.*, 2005, **62**, 2425–2430, DOI: 10.1139/f05-194.

9 M. Bizzarro, A. Simonetti, R. K. Stevenson and S. Kurszlaukis, *Geochim. Cosmochim. Acta*, 2003, **67**, 289–302, DOI: 10.1016/s0016-7037(02)01048-7.

10 F. C. Ramos, J. A. Wolff and D. L. Tollstrup, *Chem. Geol.*, 2004, **211**, 135–158, DOI: 10.1016/j.chemgeo.2004.06.025.

11 S. S. Schmidberger, A. Simonetti and D. Francis, *Chem. Geol.*, 2003, **199**, 317–329, DOI: 10.1016/s0009-2541(03)00125-6.

12 T. Waight, J. Baker and D. Peate, *Int. J. Mass Spectrom.*, 2002, **221**, 229–244, DOI: 10.1016/s1387-3806(02)01016-3.

13 J. G. Konter and L. P. Storm, *Chem. Geol.*, 2014, **385**, 26–34, DOI: 10.1016/j.chemgeo.2014.07.009.

14 J.-I. Kimura, T. Takahashi and Q. Chang, *J. Anal. At. Spectrom.*, 2013, **28**, 945–957, DOI: 10.1039/c3ja30329b.

15 Y. Tatsumi, T. Takahashi, Y. Hirahara, Q. Chang, T. Miyazaki, J.-I. Kimura, M. Ban and A. Sakayori, *J. Petrol.*, 2008, **49**, 1971–2008.

16 J.-I. Kimura, Q. Chang, K. Itano, T. Iizuka, S. B. Vaglarov and K. Tani, *J. Anal. At. Spectrom.*, 2014, DOI: 10.1039/c4ja00257a.

17 Y. H. Yang, H.-Y. Wu, J.-H. Yang, D. M. Chew, L.-W. Xie, Z.-Y. Chu, Y.-B. Zhang and C. Huang, *Chem. Geol.*, 2014, **385**, 35–55, DOI: 10.1016/j.chemgeo.2014.07.012.

18 A. V. Sovolev, A. W. Hofmann, K. P. Jochum, D. V. Kuzmin and B. Stoll, *Nature*, 2011, **476**, 434–437, DOI: 10.1038/nature10321.

19 K. P. Jochum, B. Stoll, U. Weis, D. V. Kuzmin and A. V. Sovolev, *J. Anal. At. Spectrom.*, 2009, **24**, 1237–1243, DOI: 10.1039/b905045k.

20 J.-I. Kimura, Q. Chang and H. Kawabata, *J. Anal. At. Spectrom.*, 2013, **28**, 1522–1529, DOI: 10.1039/c3ja50109d.

21 J. I. Kimua and Q. Chang, *J. Anal. At. Spectrom.*, 2012, **27**, 1549–1559, DOI: 10.1039/c2ja10344c.

22 C. Bouman, M. Deerberg and J. B. Schwieters, *Application Note Thermo Scientific*, 2009, **30187**, 1–4.

23 J. M. Koornneef, C. Bouman, J. B. Schwieters and G. R. Davies, *J. Anal. At. Spectrom.*, 2013, **28**, 749–754.

24 J.-I. Kimura, T. Nozaki, R. Senda and K. Suzuki, *J. Anal. At. Spectrom.*, 2014, **29**, 1483–1490, DOI: 10.1039/c4ja00092g.

25 T. Takahashi, Y. Hirahara, T. Miyazaki, R. Senda, Q. Chang, J.-I. Kimura and Y. Tatsumi, *J. Petrol.*, 2013, **54**, 103–148, DOI: 10.1093/petrology/egs065.

26 T. Hirata, Y. Hayano and T. Ohno, *J. Anal. At. Spectrom.*, 2003, **18**, 1283–1288.

27 K. P. Jochum, U. Nohl, K. Herwig, E. Lammel, B. Stoll and A. W. Hofmann, *Geostand. Geoanal. Res.*, 2005, **29**, 333–338.

28 J.-I. Kimura, K. Tani and Q. Chang, *Geochem. J.*, 2012, **46**, 1–12.

29 H. Kawabata, T. Hanyu, Q. Chang, J.-I. Kimura, A. R. L. Nichols and Y. Tatsumi, *J. Petrol.*, 2011, **52**, 791–838.

30 H. Bradt, in *Astrophysics Processes*, Cambridge University Press, Cambridge, 2008, p. 536.

31 M. N. Saha, *Nature*, 1920, **105**, 232–233.

32 I. Kroslakova and D. Günther, *J. Anal. At. Spectrom.*, 2007, **22**, 51–62.

33 International_Union_of_Pure_and_Applied_Chemistry, *Pure Appl. Chem.*, 1984, **56**, 695–768.

34 T. Iizuka, S. M. Eggins, M. T. McCulloch, L. P. J. Kinsley and G. E. Mortime, *Chem. Geol.*, 2011, **282**, 45–57, DOI: 10.1016/j.chemgeo.2011.01.008.

35 J. Emsley, *The Elements*, Clarendon Press, Oxford. 1998.

36 G. Horlick and Y. Shao, in *Inductively Coupled Plasma in Analytical Atomic Spectrometry*, ed. A. Montaster and D. W. Golightly, VCH Pub. Inc., New York, 2nd edn, 1992, p. 564.

37 F.-X. D'Abzac, A.-M. Seydoux-Guillaume, J. Chmeleff, L. Datas and F. Poitrasson, *J. Anal. At. Spectrom.*, 2012, **27**, 108–119, DOI: 10.1039/c1ja10145d.